AIAA JOURNAL
Vol. 33, No. 7, July 1995

Passive Damping of Truss Vibration Using Preloaded Joint Backlash

Junjiro Onoda*
Institute of Space and Astronautical Science, Sagamihara, Kanagawa 229, Japan
Tetsuji Sano†
Toyota Motor Inc., Toyota, Aichi 471, Japan
and
Kenji Minesugi‡
Institute of Space and Astronautical Science, Sagamihara, Kanagawa 229, Japan

This paper proposes using preloaded backlashes to suppress the vibration of truss structures and clarifies the vibration suppression mechanism. With preloaded backlashes, a structure keeps its high stiffness and high static shape accuracy at low external loads and vibration levels. When the response of the structure exceeds a certain level, e.g., allowable level, the joints start slipping, introducing frictional damping and nonlinearity. This nonlinearity transfers energy from lower vibration modes to higher vibration modes. Because higher mode vibrations usually damp sooner, this nonlinear transfer of energy from lower to higher modes results in a quick damping of the entire vibration. Numerical simulations show that energy transfer between the modes drastically enhances the inherent damping capability of the structure. The resulting damping can be as large as that due to the frictional force at the backlashes, even when the inherent damping ratio of each mode is only 0.2%. The simulation results demonstrate that frictional forces and enhanced inherent damping both suppress vibrations and that they are particularly effective in combination.

Introduction

LARGE structures that are deployed in space tend to be quite flexible and poorly damped since they are always made as light as possible. However, plans are being made to launch a number of payloads, such as huge space antennas and optical interferometers, for which shape accuracy is vitally important. Therefore, the suppression of vibration in space structures is an important and difficult problem.

Numerous works have been published on active vibration suppression, but the technology is still experiencing problems with instability of actively controlled systems due to phenomena such as spillover. In the case of space structures that will be constructed or deployed in orbit, it is not easy to estimate accurately the dynamic characteristics at the design phase of the control system. Such a situation makes the instability problem even harder to resolve.

Another method is passive vibration suppression. Many approaches have been proposed and investigated for the passive damping of space structures. Some of them involve using visco-elastic materials[1] or viscous fluids.[2] Others use frictional forces.[3,4] Generally speaking, passive vibration suppression methods may not be as powerful as active ones. But their simplicity, low cost, and high reliability are important advantages. Above all, they result in systems that are always stable. Even when the structures are actively controlled, passive damping plays an important role; it enhances the robustness of the system.

In some truss space structures, backlashes are almost inevitable. For example, there will almost always be some amount of clearance at the hinges of deployable structures.[5] This clearance results in backlash, which is usually regarded as detrimental because it may reduce the stiffness, shape accuracy, and linearity of the response. Therefore, some countermeasures are usually taken to eliminate backlash, such as preloading of the joints and hinges. The behavior of structures with backlashes has been studied by many researchers.[6] However, most of them have been interested in the nonlinearity of their dynamics or the elimination of their effects.

In this paper, however, we propose exploiting the nonlinear characteristics of preloaded backlashes for vibration suppression. By preloading the backlashes, we can keep high static shape accuracy provided that the vibration level, i.e., the load level, does not exceed a certain level. When the vibration level exceeds the threshold level, the backlashes start slipping, and the vibration is damped by frictional forces. In addition to the friction, we can expect another mechanism of vibration suppression, i.e., an energy shift from lower vibration modes to higher vibration modes through the nonlinearity.

Semiactive vibration suppression by stiffness control was recently proposed and studied by Onoda et al.[7] and Minesugi and Kondoh.[8] In these approaches, the energy of lower vibrational modes is transferred to higher modes by the variation of stiffness. When energy is transferred to the higher modes, quick damping of the entire vibration can be expected because the higher mode vibrations usually damp sooner. In the case of structures with preloaded backlashes, the effective stiffness decreases when the backlashes slip. Therefore, we can similarly expect the energy to transfer between the modes. Because the higher mode vibrations damp sooner, the energy of the lower modes will be transferred to the higher. As a result, we can expect damping to be enhanced by energy transfer between the modes in addition to friction.

Modeling and Formulation of Truss Structures with Backlashes

To enhance the damping of truss structures, we propose using preloaded backlashes at the joints as shown in Fig. 1, where the end of a truss member is connected to a truss node by an oval hole and a pin. The pin can move in the oval hole along the axis of the member. To eliminate the effects of backlash, it is preloaded by a spring that pushes the pin against the right end of the oval hole. The situation is essentially similar even when preloading is globally introduced to statically indeterminate structures instead of local preloading with a spring.

The characteristics of this joint can be modeled as shown in Fig. 2. Nodes l and k in the figure represent the end of the truss member

Presented as Paper 93-1549 at the AIAA/ASME/ASCE/AHS/ASC 34th Structures, Structural Dynamics, and Materials Conference, La Jolla, CA, April 19–22, 1993; received June 17, 1993; revision received March 4, 1994; accepted for publication June 21, 1994.

*Professor, Research Division of Space Transportation. Member AIAA.
†Engineer, Development Center II.
‡Associate Professor, Research Division of Space Transportation.

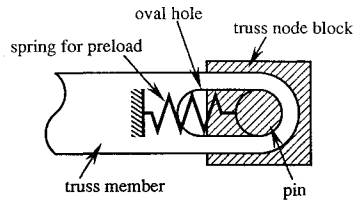

Fig. 1 Joint of truss with a backlash.

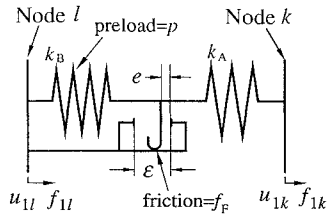

Fig. 2 Model of the backlash.

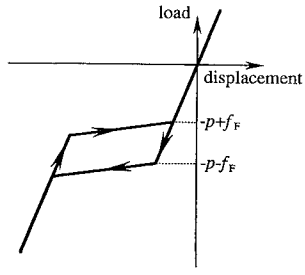

Fig. 3 Load-displacement relation of the backlash.

and the truss node, respectively. The stroke of the backlash is ε, and the frictional force is f_F. Soft spring k_B generates the compressive preload, and stiff spring k_A simulates the flexibility of the joint. When the external force is small, the backlash is eliminated by the preload p of spring k_B. As long as the compressive load on this joint does not exceed $p + f_F$, no slip occurs and the stiffness of this joint is kept at k_A. Therefore, in this situation, the stiffness is high, and the static shape accuracy is kept high. When the compressive load exceeds $p + f_F$, the truss member and the pin start to slip. When the amount of slip e does not exceed ε, the stiffness is $1/[(1/k_A) + (1/k_B)]$. When e reaches ε, the effect of backlash is again eliminated, and the stiffness will be again k_A. Thus, the load-displacement relation of the joint is as illustrated in Fig. 3.

In this paper, the finite element method is used to model a truss structure with backlashes. To simulate the behavior, including the higher modes, each truss member is divided into multiple elements. The truss members can be modeled by standard beam elements except for the end sections that have backlashes, which are modeled with special finite elements.

Each special element consists of three nodes. Let us assume that the ith element contains nodes j, k, and l as shown in Fig. 4. Node k represents a truss joint, and the section between nodes k and l represents a backlash. Although nodes k and l are shown separately in the figure, they actually occupy the same position. Node j is an intermediate node in a truss member that is connected to a standard beam element. For simplicity, the present investigation is limited to two-dimensional (or in-plane) motion. We define the nodal displacement and the nodal force of the ith element in local coordinates as

$$u_{Ei} = \lfloor u_{1j}, u_{2j}, u_{3j}, u_{1k}, u_{2k}, u_{1l} \rfloor^T \tag{1}$$

$$f_{Ei} = \lfloor f_{1j}, f_{2j}, f_{3j}, f_{1k}, f_{2k}, f_{1l} \rfloor^T \tag{2}$$

where u_{1j} and u_{2j} are the displacements in the x_{Ei} and y_{Ei} directions, respectively, u_{3j} is the rotation of node j, and x_{Ei} and y_{Ei} are the local coordinates of the ith element. Nodal forces f_{1j}, f_{2j}, and f_{3j} are the forces in the x_{Ei} and y_{Ei} directions and the moment on node j, respectively. Node l, which has been introduced to simulate the backlash, is not provided with the nodal displacement degrees of

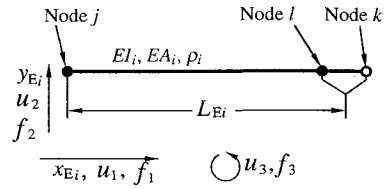

Fig. 4 Finite element simulating an end of truss member and a joint with a backlash.

freedom u_2 and u_3 because the backlash does not affect the lateral or bending displacements. Similarly, node k is not provided with the displacement degree of freedom u_3 because it is pivotal.

As the shape function for the axial displacement u_1 in the section between nodes j and l, we can use the standard linear function. For axial characteristics between nodes l and k, we assume the backlash model shown in Fig. 2, whose load-displacement relation is

$$f_i = k_{Ai}(h_i + e_i) \tag{3}$$

or

$$\begin{Bmatrix} f_{1l} \\ f_{1k} \end{Bmatrix} = k_{Ai}\begin{bmatrix} 1 & -1 \\ -1 & 1 \end{bmatrix}\begin{Bmatrix} u_{1l} \\ u_{1k} \end{Bmatrix} + k_{Ai}\begin{Bmatrix} -1 \\ 1 \end{Bmatrix} e_i \tag{4}$$

where

$$h_i = u_{1k} - u_{1l} \tag{5}$$

is the elongation of the section between nodes k and l, f_i is the load on the backlash, and e_i is the slip displacement at the backlash of the ith element as shown in Fig. 2. For the lateral displacement in the section between nodes j and k, we use the standard cubic shape function of beam elements, reflecting the fact that node k is pivotal. Then the equation of equilibrium can be obtained as

$$f_{Ei} = K_{Ei}u_{Ei} + b_{Ei}k_{Ai}e_i \tag{6}$$

where

$$K_{Ei} = \begin{bmatrix} \frac{EA_i}{L_{Ei}} & & & & & \\ 0 & \frac{3EI_i}{L_{Ei}^3} & & \text{sym} & & \\ 0 & \frac{3EI_i}{L_{Ei}^2} & \frac{3EI_i}{L_{Ei}} & & & \\ 0 & 0 & 0 & k_{Ai} & & \\ 0 & -\frac{3EI_i}{L_{Ei}^3} & -\frac{3EI_i}{L_{Ei}^2} & 0 & \frac{3EI_i}{L_{Ei}^3} & \\ -\frac{EA_i}{L_{Ei}} & 0 & 0 & -k_{Ai} & 0 & \frac{EA_i}{L_{Ei}} + k_{Ai} \end{bmatrix} \tag{7}$$

$$b_{Ei} = \lfloor 0, 0, 0, 1, 0, -1 \rfloor^T \tag{8}$$

and where EA_i is the axial stiffness, EI_i is the bending stiffness, and L_{Ei} is the length of the ith element. By using the aforementioned shape functions, one can also derive a consistent mass matrix from the standard procedure. Because e_i is an independent variable, another equation that describes the behavior of e_i is still required.

For simplicity, let us assume that the static and dynamic frictional forces at the backlash are identical. Then we can see that the slip at the backlash does not start in the ith element when the inequality

$$|p_i + (k_{Ai} + k_{Bi})e_i + k_{Ai}h_i| < f_{Fi} \tag{9}$$

is satisfied, where f_{Fi} is the frictional force and p_i is the preload of the ith element, respectively. In addition, the slip is limited to the range

$$0 \le e_i \le \varepsilon_i \tag{10}$$

Therefore, slip does not occur when either of the following conditions holds:

$$e_i = 0 \quad \text{and} \quad p_i + (k_{Ai} + k_{Bi})e_i + k_{Ai}h_i \geq f_{Fi} \tag{11}$$

$$e_i = \varepsilon_i \quad \text{and} \quad p_i + (k_{Ai} + k_{Bi})e_i + k_{Ai}h_i \leq -f_{Fi} \tag{12}$$

When the inequalities are about to be violated, the slip starts. Because the frictional force is f_{Fi} when the backlash is slipping, we can see that

$$|p_i + (k_{Ai} + k_{Bi})e_i + k_{Ai}h_i| = f_{Fi} \tag{13}$$

Therefore, when the backlash is slipping, the value of e_i can be obtained from the following equations:

$$e_i(k_{Ai} + k_{Bi}) + k_{Ai}h_i + p_i + f_{Fi} = 0 \qquad \text{when } \dot{e}_i > 0 \tag{14}$$

$$e_i(k_{Ai} + k_{Bi}) + k_{Ai}h_i + p_i - f_{Fi} = 0 \qquad \text{when } \dot{e}_i < 0 \tag{15}$$

By transforming into global coordinates and assembling the stiffness matrices and mass matrices of all of the elements, we can obtain the equations of motion as

$$M\ddot{u} + Ku + BGe = 0 \tag{16}$$

where

$$B = [b_1, b_2, \ldots, b_{n_b}] \tag{17}$$

$$G = \text{diag}[k_{Ai}] \tag{18}$$

$$e = \lfloor e_1, e_2, \ldots, e_{n_b} \rfloor^T \tag{19}$$

$$b_i = T_i b_{Ei} \tag{20}$$

Matrices M and K are the mass and stiffness matrices of the total system, respectively, u is the nodal displacement vector in the global coordinates, n_b is the number of backlashes, and T_i is a transfer matrix from the displacement vector of the ith element in local coordinates to the global displacement vector of the total degrees of freedom. From the definition, we can see that

$$h_i = b_i^T u \tag{21}$$

It is known that the per-cycle energy loss due to structural damping is usually independent of frequency.[9] A standard procedure to take this type of structural damping into account is to replace k_{Ai}, K_{Ei}, k_{Bi}, K, and G in Eqs. (3), (4), (6), (9), and (11–16) with

$$k_{Ai}\left(1 + \frac{2\zeta}{\omega}\frac{\mathrm{d}}{\mathrm{d}t}\right), \qquad K_{Ei}\left(1 + \frac{2\zeta}{\omega}\frac{\mathrm{d}}{\mathrm{d}t}\right), \qquad k_{Bi}\left(1 + \frac{2\zeta}{\omega}\frac{\mathrm{d}}{\mathrm{d}t}\right)$$

$$K\left(1 + \frac{2\zeta}{\omega}\frac{\mathrm{d}}{\mathrm{d}t}\right), \quad \text{and} \quad G\left(1 + \frac{2\zeta}{\omega}\frac{\mathrm{d}}{\mathrm{d}t}\right)$$

respectively, where ω is the angular frequency, ζ is the damping ratio, and t is time. Consequently, Eqs. (16) and (3) [after substituting Eq. (21)] result in

$$M\ddot{u} + K\left(u + \frac{2\zeta}{\omega}\dot{u}\right) + BG\left(e + \frac{2\zeta}{\omega}\dot{e}\right) = 0 \tag{16'}$$

$$f_i = k_{Ai}\left[b_i^T\left(u + \frac{2\zeta}{\omega}\dot{u}\right) + e_i + \frac{2\zeta}{\omega}\dot{e}_i\right] \tag{3'}$$

Although this approximation does not represent the true damping laws, it is a better approximation than viscous damping in many cases.[9]

Let us transform Eq. (16′) into modal coordinates as

$$\ddot{q} + 2\zeta D\dot{q} + \Omega q + \frac{1}{m_N}\Phi^T BG(e + C\dot{e}) = 0 \tag{22}$$

where

$$u = \Phi q \tag{23}$$

$$\Omega = \text{diag}\left[\omega_i^2\right] \tag{24}$$

$$D = \text{diag}[\omega_i] \tag{25}$$

$$\Phi = [\phi_1, \phi_2, \ldots, \phi_n] \tag{26}$$

$$C = \text{diag}[2\zeta/\omega_{\text{eff},i}] \tag{27}$$

$$m_N = \phi_i^T M \phi_i \tag{28}$$

and where q is the displacement vector in modal coordinates, ω_i and ϕ_i are the angular frequency and mode shape of the ith mode under the condition that no backlash slips, respectively, m_N is a normalizing mass, and $\omega_{\text{eff},i}$ is the effective angular frequency of the ith backlash whose value is to be determined in the following paragraph.

Equation (25) is a standard approximation, which is equivalent to assuming an identical damping ratio for all of the modes. In the derivation of Eq. (25), the value of ω in the second term of Eq. (16′) for the ith mode velocity component is assumed to be ω_i, resulting in

$$\phi_i^T \frac{1}{\omega} K \phi_i = \omega_i \tag{29}$$

To be consistent with this assumption and Eq. (27), Eq. (3′) has to be

$$f_i = k_{Ai}\left[b_i^T\left(\sum_{j=1}^{n}\phi_j q_j + \sum_{j=1}^{n}\frac{2\zeta}{\omega_j}\phi_j\dot{q}_j\right) + e_i + \frac{2\zeta}{\omega_{\text{eff},i}}\dot{e}_i\right] \tag{30}$$

When

$$\dot{u}_{1k} - \dot{u}_{1l} + \dot{e}_i = b_i^T \sum_{j=1}^{n}\phi_j\dot{q}_j + \dot{e}_i = 0 \tag{31}$$

holds, spring k_A is neither elongating nor contracting. Therefore, in such a situation, the axial load on the backlash should be independent of the velocity terms, resulting in

$$f_i = k_{Ai} b_i^T\left(\sum_{j=1}^{n}\phi_j q_j + e_i\right) \tag{32}$$

To satisfy Eq. (32) under the condition stated in Eq. (31), $\omega_{\text{eff},i}$ has to be

$$\omega_{\text{eff},i} = \left(b_i^T \sum_{j=1}^{n}\phi_j\dot{q}_j\right) \Big/ \left(b_i^T \sum_{j=1}^{n}\frac{1}{\omega_j}\phi_j\dot{q}_j\right) \tag{33}$$

In this paper, $\omega_{\text{eff},i}$ is approximated as Eq. (33) with the constraint

$$\omega_{\text{eff},i} \geq 0 \tag{34}$$

In the modal coordinates, Eqs. (9), (11), (12), (14), and (15) can be rewritten as follows after introduction of structural damping:

$$\left|p_i + (k_{Ai} + k_{Bi})\left(e_i + \frac{2\zeta}{\omega_{\text{eff},i}}\dot{e}_i\right) + k_{Ai}b_i^T\sum_{j=1}^{n}\left(q_j + 2\zeta\frac{\dot{q}_j}{\omega_j}\right)\phi_j\right| < f_{Fi} \tag{9'}$$

$$e_i = 0 \quad \text{and} \quad p_i + (k_{Ai} + k_{Bi})\left(e_i + \frac{2\zeta}{\omega_{\text{eff},i}}\dot{e}_i\right) + k_{Ai}b_i^T\sum_{j=1}^{n}\left(q_j + 2\zeta\frac{\dot{q}_j}{\omega_j}\right)\phi_j \geq f_{Fi} \tag{11'}$$

$$e_i = \varepsilon_i \quad \text{and} \quad p_i + (k_{Ai} + k_{Bi})\left(e_i + \frac{2\zeta}{\omega_{\text{eff},i}}\dot{e}_i\right) + k_{Ai}b_i^T \sum_{j=1}^{n}\left(q_j + 2\zeta\frac{\dot{q}_j}{\omega_j}\right)\phi_j \le f_{Fi} \tag{12'}$$

$$(k_{Ai} + k_{Bi})\left(e_i + \frac{2\zeta}{\omega_{\text{eff},i}}\dot{e}_i\right) + k_{Ai}b_i^T \sum_{j=1}^{n}\left(q_j + 2\zeta\frac{\dot{q}_j}{\omega_j}\right)\phi_j + p_i + f_{Fi} = 0 \quad \text{when } \dot{e}_i > 0 \tag{14'}$$

$$(k_{Ai} + k_{Bi})\left(e_i + \frac{2\zeta}{\omega_{\text{eff},i}}\dot{e}_i\right) + k_{Ai}b_i^T \sum_{j=1}^{n}\left(q_j + 2\zeta\frac{\dot{q}_j}{\omega_j}\right)\phi_j + p_i - f_{Fi} = 0 \quad \text{when } \dot{e}_i < 0 \tag{15'}$$

The ith backlash does not slip when any of Eqs. (9'), (11'), or (12') hold. Otherwise the backlash slips, and the value of e_i can be obtained from Eqs. (14') and (15'). These equations and Eq. (22) compose the complete set of equations of motion.

Numerical Simulation and Investigation of Damping Due to Backlashes

To investigate how the backlashes contribute to damping, the in-plane truss structure shown in Fig. 5 is studied as an example. The length of the nondiagonal truss members is L_M. All of the members have mass per unit length ρ, axial stiffness EA, and bending stiffness EI. As shown in the figure, the truss structure has three identical backlashes with stroke ε, preload p, frictional force f_F, spring constant for preload k_B, and joint flexibility k_A. The mass of each truss node is ρL_M.

In the numerical simulation, each truss member is modeled by three finite elements. In the modal equations of motion, 87 modes are kept without any truncation of modes. The damping ratio of all of the modes is assumed to be ζ. An impulse of amplitude Δ is applied to a truss node as shown in Fig. 5, and the subsequent motion is simulated. The modified Euler method[10] is used to integrate the equations of motion. In the following examples, the following parameter values are used:

$$\varepsilon = 0.001L_M, \qquad k_B/(EA/L_M) = 0.001$$
$$k_A/(EA/L_M) = 1000, \qquad EI/(EAL_M^2) = 1 \times 10^{-3}$$

Except for the case shown in Fig. 6, the preload is assumed as

$$p/(EA) = 1 \times 10^{-5}$$

and the intensity of the impulse is assumed as follows (except for the cases shown in Fig. 13):

$$\Delta/\sqrt{EAm_TL_M} = 0.001$$

where m_T is the total mass of the structure, i.e., $(15 + 3\sqrt{2})\rho L_M$.

Figures 6–10 show some simulation results. These figures show the time histories of the first modal displacement q_1, the root-mean-square (rms) displacements of the truss nodes u_{rms}, the amount of slip in the first backlash e_1, and the total energy T, respectively, in the following normalized forms:

$$\tilde{q}_1 \equiv \frac{q_1}{\Delta}\sqrt{\frac{EAm_T}{L_M}} \tag{35}$$

$$\tilde{u}_{\text{rms}} \equiv \frac{u_{\text{rms}}}{\Delta}\sqrt{\frac{EAm_T}{L_M}} \tag{36}$$

$$\tilde{T} = Tm_T/\Delta^2 \tag{37}$$

Results Using High Preload

Figure 6 shows the case where the preload is so large that the effects of the backlashes are completely eliminated. The value of e_1 is not shown in the figure because it stays at zero. The inherent structural damping ratio is $\zeta = 0.002$. Because of the low inherent damping, the vibration damps slowly, and both the rms displacement and the total energy decrease slowly. Because the higher modes excited by the impulse damp sooner, the total energy and the rms displacement decreases faster than the first mode amplitude, especially in the initial phase.

Results Without Inherent Damping and Friction

Figure 7 shows the case where the inherent damping and the friction are both zero, i.e., $\zeta = 0$, and $f_F = 0$. The preload is $p = 1 \times 10^{-5}EA$, and the backlashes are effective. Because there is no inherent damping or friction in the system, the total energy remains constant, and no energy dissipates as shown in Fig. 7d. The figure shows that no artificial damping is introduced by, for example, numerical calculation errors. Because of the energy transfer between the modes, the amplitude of the first mode and the rms displacement fluctuate as shown in Figs. 7a and 7b.

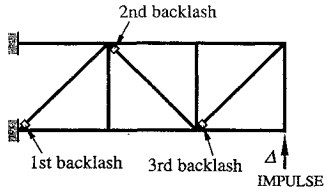

Fig. 5 Two-dimensional truss with backlashes.

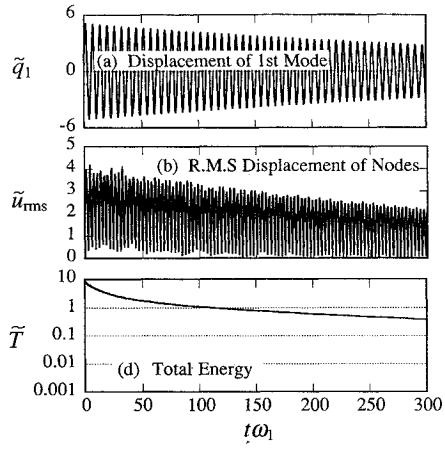

Fig. 6 Simulation result (no effects of backlashes due to large preload); $\zeta = 0.002$, $f_F = 0$, and $p = EA$.

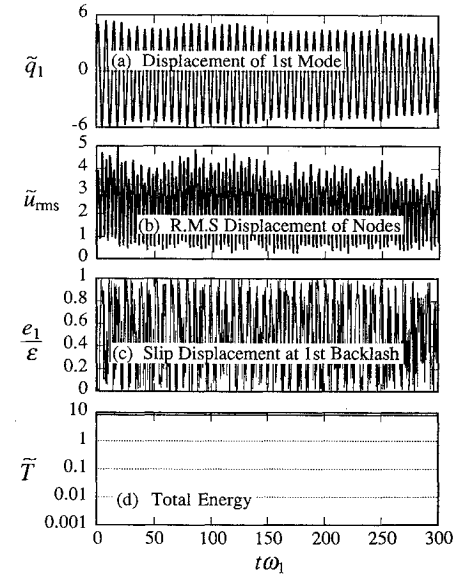

Fig. 7 Simulation result (no inherent damping and no friction); $\zeta = 0$, $f_F = 0$, and $p = 1 \times 10^{-5}EA$.

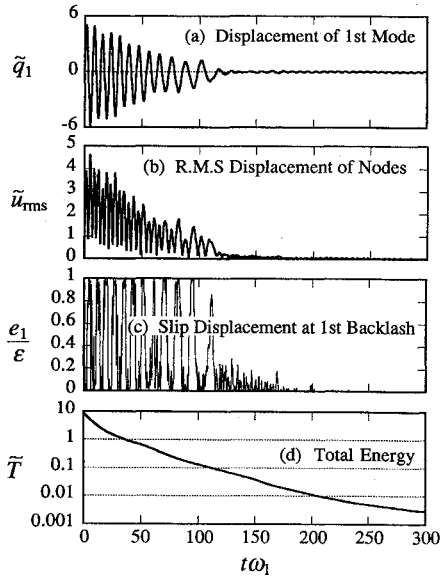

Fig. 8 Simulation result (no friction); $\zeta = 0.002, f_F = 0$, and $p = 1 \times 10^{-5}EA$.

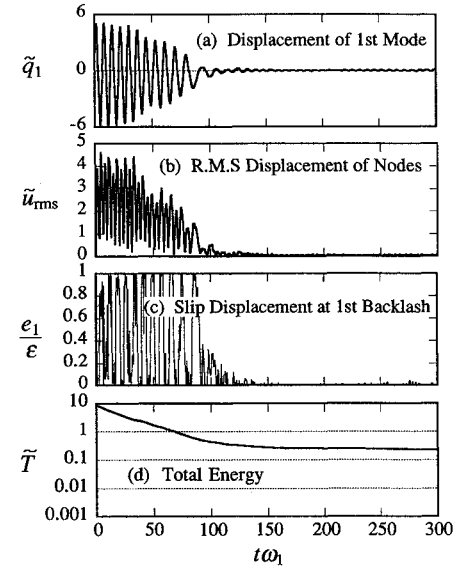

Fig. 9 Simulation result (no inherent damping); $\zeta = 0, f_F = 1 \times 10^{-5}EA$, and $p = 1 \times 10^{-5}EA$.

Results with Inherent Damping and Without Friction

When a small amount of inherent damping is introduced into the system whose response is shown in Fig. 7, the response changes to that shown in Fig. 8, where the parameter values are the same as those of Fig. 7 except that $\zeta = 0.002$. Figure 8a shows that the first mode vibration is suppressed nicely. Figure 8b shows that the rms displacement also decreases quickly. Figure 8d shows that the total energy dissipates much more quickly than in Fig. 6d, even though the values of ζ of these two system (Figs. 6 and 8) are identical, and no other energy dissipation mechanisms exist in them. Therefore, we can see that the rapid energy dissipation of Fig. 8d is entirely due to the enhancement of inherent damping by the backlashes. Comparison of Figs. 8 and 6 clearly shows that the energy dissipation capability can be drastically enhanced by the backlashes.

Results Without Inherent Damping and with Friction

Figure 9 shows the case where friction exists, and the inherent damping is zero, i.e., $\zeta = 0$, and $f_F = 1.0 \times 10^{-5}EA$. In this case, the total energy dissipation is fully due to frictional forces. The figure shows that friction also dissipates the energy and reduces the vibration amplitude well. However, the figure shows that the energy ceases to dissipate as soon as the slip at the backlash stops.

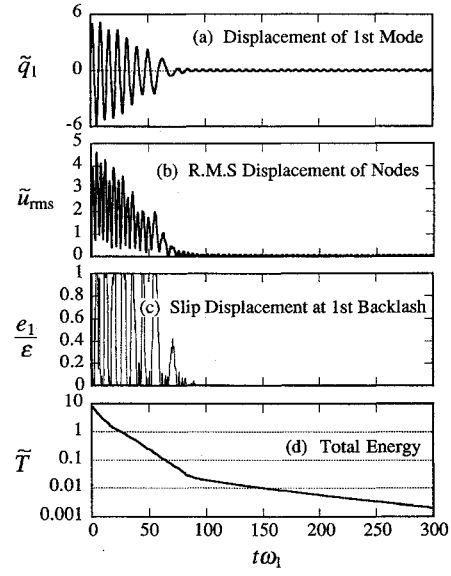

Fig. 10 Simulation result (with both the inherent damping and the friction); $\zeta = 0.002, f_F = 1 \times 10^{-5}EA$, and $p = 1 \times 10^{-5}EA$.

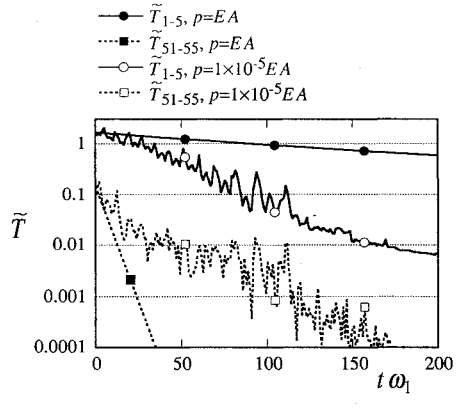

Fig. 11 Time history examples of the energies of lower modes and higher modes.

Results with Inherent Damping and Friction

Figure 10 shows the cases where both inherent damping and frictional forces exist, i.e., $\zeta = 0.002$, and $f_F = 1.0 \times 10^{-5}EA$. The total energy, rms displacement, and the amplitude of the first mode decrease more rapidly than in Figs. 8 and 9 due to both the frictional force and the enhancement of inherent damping by the backlashes.

Energy Transfer and Dissipation

It is difficult to define the energy of each vibration mode of the system under study in a strict sense unless all of the values of e_i are zero. However, the value of

$$T_i = \omega_i^2 q_i^2 + \dot{q}_i^2 \tag{38}$$

represents the energy of the ith mode when all e_i are zero. Even when some of e_i are not zero, it roughly represents the intensity of the ith mode vibration. Therefore, let us call it "energy of the ith mode" tentatively in this paragraph. Figure 11 shows the time histories of the energies of the lowest five modes and the higher modes, i.e., $\tilde{T}_{1-5}$ (solid lines) and $\tilde{T}_{51-55}$ (dotted lines), where

$$\tilde{T}_{k-l} = \left(\sum_{i=k}^{l} T_i \right) m_T / \Delta^2 \tag{39}$$

The figure shows that when the backlashes are not effective because of the excessive preload ($p = EA$), the energies of the lowest five modes and the higher modes (from the 51st to the 55th modes) decrease monotonically. It also shows that the energy of the higher modes decreases much faster than that of the lower modes. However,

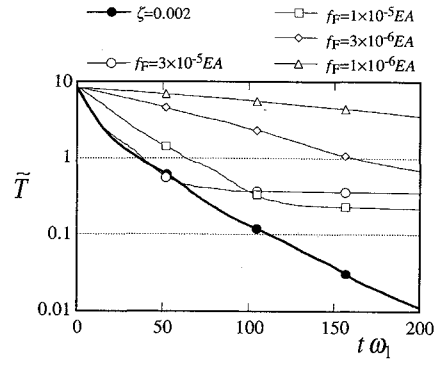

Fig. 12 Time histories of total energy; $p = 1 \times 10^{-5}EA$.

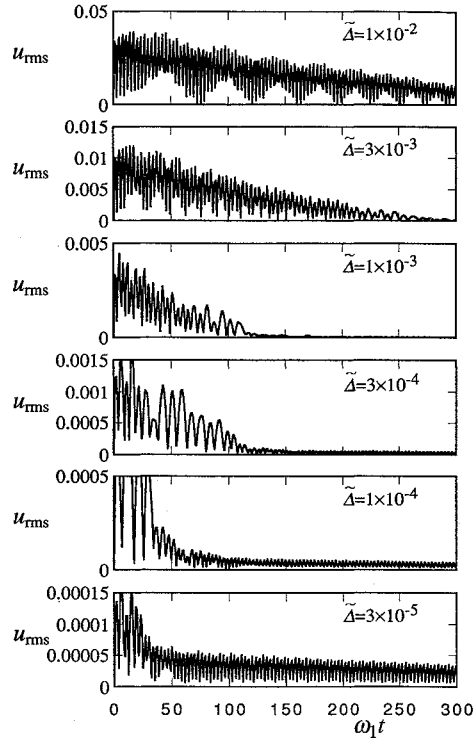

Fig. 13 Effect of the impulse level on the response of the structure with backlashes.

when the backlashes are effective ($p = 10^{-5}EA$), the energy of the higher modes decreases more slowly, and that of the lowest modes decreases more rapidly than the case where $p = EA$, respectively. This fact indicates that the energy of the lowest modes (which otherwise decreases slowly) is transferred to the higher modes (which decreases rapidly) by the effect of the backlashes. Consequently, this energy transfer results in a rapid damping of the entire vibration.

Figure 12 shows the time histories of total energy for various parameter values. The thick line shows the case where no friction exists, and only enhanced inherent damping dissipates the energy. The thin lines are the cases where no inherent damping exists, and only friction dissipates the energy. The figure shows that the energy dissipation at the initial phase due to the frictional force is large when the frictional force is large. However, the larger the frictional force, the more energy that remains when the energy ceases decreasing. This trend is the same as shown in Ref. 4. When the frictional force is larger than the preload, i.e., $f_F > p$, it is possible that the backlash will stick at a nonzero position and that the value of e will remain nonzero after the decay of vibration, resulting in a static distortion. Therefore, it is not practical to make the frictional force larger than the preload even though the initial energy dissipation rate is high. From this point of view, the figure shows that the energy dissipation due to inherent damping enhanced by backlashes can be larger than that due to friction even when the inherent damping ratio is as small as 0.2%.

Effects of Impulse Intensity

Figure 13 shows the effect of the impulse intensity on the response or the time history of rms displacement. In all of the cases shown in Fig. 13, the parameter values are

$$f_F = 0, \qquad p/EA = 10^{-5}, \qquad \zeta = 2 \times 10^{-3}$$

The figure shows that the damping capability of the structure with backlashes is excellent only when the impulse level is adequate, although its adequate range is wider than one order of magnitude. In other words, it is important to select the parameter values of the backlashes suitably to make the backlashes effective for given impulse levels. This figure suggests that we can design a structure with backlashes whose damping becomes large when the vibration level is about to exceed a given limit.

Additional Investigation

In the preceding investigation, structural damping was taken into account based on the approximations of Eqs. (25) and (27). Some may feel uncomfortable with Eq. (27) because of the introduction of $\omega_{\text{eff},i}$. A possible way to avoid the introduction of $\omega_{\text{eff},i}$ is to assume that the springs k_A and k_B have no inherent damping. Because this assumption will result in an underestimation of the damping capability, we can still demonstrate the damping enhancement of the original system by showing the damping enhancement under this assumption. If the spring k_A has no inherent damping, Eq. (16′) becomes

$$M\ddot{u} + (2\zeta/\omega)K^{-}\dot{u} + Ku + BGe = 0 \qquad (16'')$$

and Eq. (30) becomes the same as Eq. (32), where K^{-} is a stiffness matrix that does not include the stiffness of spring k_A of all of the backlashes. Therefore, it is not necessary to introduce $\omega_{\text{eff},i}$ under this assumption. Equation (16″) can be transformed into modal coordinates as

$$\ddot{q} + 2(\zeta/\omega)\Phi^T K^{-}\Phi\dot{q} + \Omega q + (1/m_N)\Phi^T BGe = 0 \qquad (22')$$

and all of the terms of $2\zeta/\omega_{\text{eff},i}$ in Eqs. (9′), (11′), (12′), (14′), and (15′) disappear.

Because K^{-} is different from K, $\Phi^T K^{-}\Phi$ is not a diagonal matrix. In such a case, it is not clear what value ω represents, and again we have to make an approximation for the value of ω in the second term of Eq. (22′). There are three candidates for this approximation:

$$D'_{ij} = (1/\omega_i)\phi_i^T K^{-}\phi_j \qquad (40)$$

$$D'_{ij} = (1/\sqrt{\omega_i\omega_j})\phi_j^T K^{-}\phi_j \qquad (41)$$

$$D'_{ij} = (1/\omega_j)\phi_i^T K^{-}\phi_j \qquad (42)$$

where D'_{ij} is the ith-row jth-column element of matrix D' defined as

$$D' = (1/\omega)\Phi^T K^{-}\Phi \qquad (43)$$

Based on Eqs. (22′), (32), and (40–43), we performed some numerical simulations of the motion of the truss structure subsequent to the impulse. Figure 14 compares the time histories of the total energy obtained from the numerical simulations based on

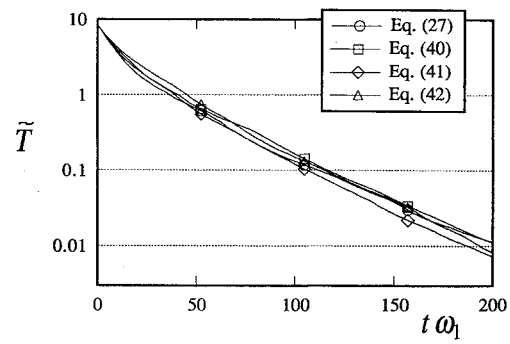

Fig. 14 Comparison of time histories of total energy from four different approximations.

these three approximations, i.e., Eqs. (40–42), with that based on the approximation Eq. (27). The figure shows that the difference between these four time histories is insignificant, suggesting that these approximations are acceptable for the purpose of this paper, which is to demonstrate the effectiveness of enhanced inherent damping.

Concluding Remarks

To suppress the vibration of space truss structures, a passive approach has been proposed and investigated. This approach involves using preloaded backlashes in the structures.

Numerical simulations have shown that energy transfer between the modes drastically enhances the inherent damping capability of the structure, even when no friction exists at the backlashes. The resulting damping can be as large as that due to the frictional force at the backlashes even when the inherent damping ratio of each mode is as low as 0.2%. Simulation results have demonstrated that the combination of frictional forces and enhanced inherent damping suppress vibrations very effectively.

In this investigation, the damping ratio of each mode was assumed to be identical. This assumption guarantees that the higher modes damp sooner and forms the basis of the damping enhancement mechanism. Generally, this assumption may not be true in actual structures, but we can expect enhancement of the inherent damping if the values of $\zeta\omega$ of most of the higher modes are higher than those of the lower modes. This seems to be true in the majority of actual structures.

References

[1]Barrett, D. J., "A Design for Improving the Structural Damping Properties of Axial Members," *Proc. Damping'89*, Wright–Patterson AFB, OH, WRDC-TR-89-3116, Volume 3, Paper HCB, Feb. 1989.

[2]Davis, L. P., Workman, B. J., Chu, C.-C., and Anderson, E. H., "Design of a D-Strut and Its Application Results in the JPL, MIT, and LARC Test Bed," *Proceedings of the AIAA/ASME/ASCE/AHS/ASC 33rd Structure, Structural Dynamics, and Materials Conference*, AIAA, Washington, DC, 1992, pp. 1524–1530 (AIAA Paper 92-2274).

[3]Meng, C. H., Chidamparam, P., and Griffin, J. H., "Friction Damping of Two-Dimensional Motion and Its Application in Vibration Control," *Journal of Sound and Vibration*, Vol. 144, No. 3, 1991, pp. 427–447.

[4]Onoda, J., and Minesugi, K., "Semi-Active Vibration Suppression of Truss Structures by Coulomb Friction," *Proceedings of the AIAA/ASME/ASCE/AHS/ASC 33rd Structure, Structural Dynamics, and Materials Conference*, AIAA, Washington, DC, 1992, pp. 1488–1496 (AIAA Paper 92-2270); see also *Journal of Spacecraft and Rockets*, Vol. 31, No. 1, 1994, pp. 67–74.

[5]Onoda, J., "Two-Dimensional Deployable Truss Structures for Space Applications," *Journal of Spacecraft and Rockets*, Vol. 25, No. 2, 1988, pp. 109–116.

[6]Shi, G., and Atluri, S. N., "Nonlinear Dynamic Response of Frame-Type Structures with Hysteric Damping at Joints," *AIAA Journal*, Vol. 30, No. 1, 1992, pp. 234–240.

[7]Onoda, J., Endo, T., Tamaoki, H., and Watanabe, N., "Vibration Suppression by Variable-Stiffness Members," *AIAA Journal*, Vol. 29, No. 6, 1991, pp. 977–983.

[8]Minesugi, K., and Kondoh, K., "Semi-Active Vibration Suppression of Large Space Structures with a Variable Axial Stiffness Member," *Proceedings of the AIAA/ASME/ASCE/AHS/ASC 34th Structure, Structural Dynamics, and Materials Conference*, AIAA, Washington, DC, 1993, pp. 3305–3311 (AIAA Paper 93-1693).

[9]Bishop, R. E. D., and Johnson, D. C., *The Mechanics of Vibration*, Cambridge Univ. Press, Cambridge, England, UK, 1960, Chap. 9.

[10]Hahn, G. D., "A Modified Euler Method for Dynamic Analyses," *International Journal for Numerical Methods in Engineering*, Vol. 32, No. 5, 1991, pp. 943–955.